JGR Solid Earth

RESEARCH ARTICLE
10.1029/2021JB022755

Analyzing Bulk Flow Characteristics of Debris Flows Using Their High Frequency Seismic Signature

Zhen Zhang[1,2,3], Fabian Walter[2,4], Brian W. McArdell[4], Tjalling de Haas[5], Michaela Wenner[2,4], Małgorzata Chmiel[2], and Siming He[1,3]

[1]Institute of Mountain Hazards and Environment, Chinese Academy of Sciences, Chengdu, China, [2]Laboratory of Hydraulics, Hydrology and Glaciology, ETH Zürich, Zürich, Switzerland, [3]University of Chinese Academy of Sciences, Beijing, China, [4]Swiss Federal Institute for Forest, Snow and Landscape Research WSL, Birmensdorf, Switzerland, [5]Department of Physical Geography, Universiteit Utrecht, Utrecht, The Netherlands

Key Points:

- We extend the single-particle impact model to multi-particle force chains generating debris-flow seismic signals
- Theoretically predicted basal force fluctuations are consistent with in-situ measurements and inverted results from seismic signals
- Both single-particle impacts and multi-particle force chain impacts control basal force fluctuations

Supporting Information:

Supporting Information may be found in the online version of this article.

Correspondence to:

Z. Zhang and S. He,
zhangzhenkgands@163.com;
hsm@imde.ac.cn

Citation:

Zhang, Z., Walter, F., McArdell, B. W., de Haas, T., Wenner, M., Chmiel, M., & He, S. (2021). Analyzing bulk flow characteristics of debris flows using their high frequency seismic signature. *Journal of Geophysical Research: Solid Earth*, *126*, e2021JB022755. https://doi.org/10.1029/2021JB022755

Received 9 JUL 2021
Accepted 12 DEC 2021

Abstract Quantifying debris-flow characteristics remains a key challenge in natural hazard research. Recent studies suggest that seismic signals can reveal debris-flow properties. However, the accuracy and applicability of theoretical models linking bulk flow properties to the seismic signature of a debris flow remain elusive. By extending a previously proposed model of random single-particle impact forces to multi-particle force chains acting on the channel bed, we describe the generation of high frequency seismic signals, and thereby estimate the bulk flow dynamics of six debris-flow events at Illgraben, Switzerland. The theoretically predicted basal force fluctuations agree with in-situ measurements at a basal force plate and seismic signals recorded adjacent to the channel. According to our model, both random single-particle impacts and random impacts caused by multi-particle force chains control basal force fluctuations. The relative contributions of single particles and of multi-particle force chains may vary significantly for different events and different positions within events. The relative contribution of multi-particle force chains is expected to be larger in the flow front, where particle concentrations are higher. The ratio between single-particle and multi-particle contributions appears to control the non-linear relation between flow depth and the magnitude of the high frequency seismic signals. Our results suggest that fluctuating basal forces are strongly controlled by particle size and flow depth, and open new perspectives for the understanding of bulk flow characteristics, such as flow depth and weight, and of the high frequency seismic signals generated by debris flows.

Plain Language Summary Traditional methods have many limitations in observing and estimating debris-flow characteristics, such as flow depth and weight. Although an increasing number of studies has recently shown the potential of using seismic signals to observe these debris-flow characteristics, the physical relation between these characteristics and ground vibrations is not well understood. Here we develop a model, which describes how particles within a debris flow transmit forces as they collide with the ground. We focus on six debris flows at Illgraben, Switzerland, and observe a good agreement between modeled and measured forces. We find that both multi-particle force chain impacts and single-particle impacts control the debris-flow basal force fluctuations. Thicker flows transmit more seismic energy to the underlying ground. Our study shows how seismic measurements can be used to obtain quantitative information about debris flows.

1. Introduction

Understanding the dynamics of debris flows is essential for early warning system design, damage reduction, and modeling landscape evolution. The sudden onset of debris flows, and their unpredictable and destructive character, inhibit direct field measurements of flow characteristics. Yet, recent studies showed that seismic signals contain information on flow characteristics of natural mass movements, such as landslides, rockfalls, and debris flows (e.g., Allstadt et al., 2018; Ekström & Stark, 2013; Walter et al., 2020; Zhang & He, 2019).

Much seismological debris-flow research has focused on event detection and early warning, rather than analyzing debris-flow dynamics (e.g., Chmiel et al., 2021; Coviello et al., 2019; Schimmel & Hübl, 2015, 2016; Schmandt et al., 2013; Walter et al., 2017). However, developing a physical model of the seismic signature of debris flows that can describe the generation of dominant high frequencies (>1 Hz) is still a challenge. The typical high frequency seismic signals generated by debris flows are sensitive to small-scale ground heterogeneity near the surface (Allstadt, 2013; Hibert et al., 2017; Ogiso & Yomogida, 2015; Tsai et al., 2012). To isolate seismic sources

within the debris flow, seismic propagation effects need to be deconvolved from the recorded seismograms. Seismic path effects of high frequency signals can be estimated using empirical Green's functions (Allstadt et al., 2020) or seismic ground models (Zhang et al., 2021).

The temporal flow patterns of debris flows are complex, which complicates formulation of seismic source models linking seismic signals to flow characteristics. Temporal changes in flow depth, mass density, and flow velocity of the debris material are likely too slow to affect high frequency seismic signals on the order of several Hz or greater, which are the frequencies typically recorded in close proximity to debris flows (Allstadt et al., 2020). Most existing theoretical descriptions of high frequency debris-flow seismicity are based on the bedload transport model by Tsai et al. (2012), henceforth referred to as the "Tsai model". This model allows estimation of debris-flow entrainment and the effective particle diameter using seismic recordings (Kean et al., 2015; Lai et al., 2018). Furthermore, it provides a relation between peak signal frequency and source-to-receiver distance, which can improve debris-flow warning (Lai et al., 2018). The predictions of the Tsai model rely on the idea that high frequency seismic signals are proportional to force fluctuations generated by stochastic particle impacts on the bed, although some modifications, specifically in the context of debris flows, have been proposed (Farin et al., 2019). Seismic signal generation via force transmission into the channel bed is a well-accepted concept and the Tsai model uses it to link a number of debris-flow properties to high frequency seismic signals. However, although various models based on the Tsai et al. (2012) paradigm have been tested against laboratory experimental data (Arran et al., 2021; de Haas et al., 2021), these models have not yet been thoroughly verified against independent field data (Allstadt et al., 2020; Zhang et al., 2021).

Besides impact forces, other debris-flow processes may change over short time scales to produce high frequency seismic signals: dense particle concentration favors formation of force chains (Campbell, 2006; Majmudar & Behringer, 2005; Muthuswamy & Tordesillas, 2006), which transmit collision forces within the flow to the bed. As the flow density increases, the inter-particle forces in debris materials are expected to form a distributive network of filamentary force-accommodating chains (i.e., force chains; Estep & Dufek, 2012). The force of each contact in a force chain can be transmitted to the basal substrate via the particles, which are in contact with each other, thereby causing local basal forces many times greater than the weight of the single particle (Berhringer et al., 2008; Estep & Dufek, 2012; Furbish et al., 2008; Majmudar et al., 2007). The production and disruption of force chains within flowing debris materials are expected to occur rapidly (Furbish et al., 2008), and to cause significant basal force fluctuations in flows with high particle concentrations.

Besides force chains, the interactions of particle clusters with the bed can generate basal force fluctuations (Iverson, 1997; Iverson & LaHusen, 1989). However, seismic radiation is likely minor because clustering is expected to only affect the smallest size particles (Lamb et al., 2008). For the present study we also ignore dynamic pore-pressure fluctuations and the influence of fluid-bed interactions within debris materials in the flow front, because for events at our study site (Illgraben, Switzerland), coarse debris-flow fronts have rather low mean fluid pressures which are somewhat smaller than the mean pressures generated by the entire flow (McArdell et al., 2007).

In general, force transmission other than stochastic particle impacts may contribute to high frequency seismic signal generation. It is therefore not clear to what extent observed scaling relations between high frequency seismic signals and bulk flow characteristics (such as local flow depth, flow weight, and bulk kinetic energy; Allstadt et al., 2020; Coviello et al., 2019; Hsu et al., 2014; McCoy et al., 2013) can be explained with existing theoretical models.

To address these questions, we propose an extended physical model consisting of both multi-particle force chains and the random single-particle impacts that have been previously modeled. This provides a quantitative explanation for relations between high frequency debris-flow seismicity and bulk flow characteristics. We calculate basal force fluctuations on the torrent bed using seismological observations of six well-documented debris flows at Illgraben, Switzerland. Verified against independent measurements from a large basal force plate, our inverted basal fluctuations correlate with the bulk properties of the flow, including flow depth and weight.

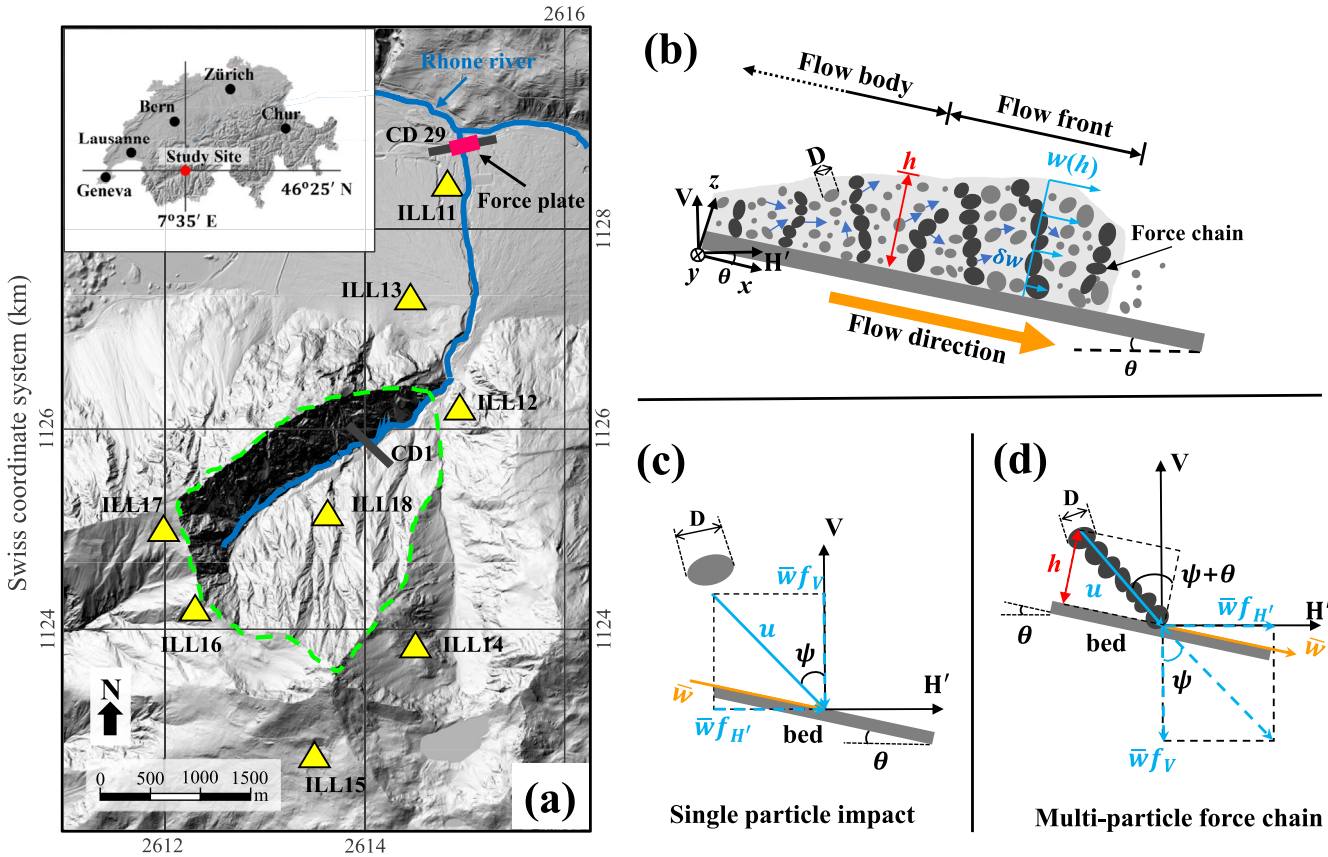

Figure 1. Study site. (a) Illgraben catchment (location in Switzerland is marked by the red dot in the inset map) with dashed green line outlining the upper catchment. Solid blue lines represent the Illgraben torrent and the Rhone River. Yellow triangles represent locations of seismic stations. The magenta rectangle indicates the location of the force plate. Black bars are the locations of selected check dams (CD). (b) Conceptual model of a debris flow. Schematics of a particle (c) (diameter D) and force chain (d) impact on the bed showing the relevant angles. h is the flow depth. x, y, and z represent the downslope, transverse, and normal directions, respectively. V and H represent vertical and the vector sum of the two orthogonal horizontal directions, respectively. H′ represents the projection of horizontal direction H on the x–z plane. See main text for definition of velocities $w(h)$, δw, and $\overline{w}$, and dimensionless function f_i.

2. Study Site and Data

The Illgraben catchment in southwestern Switzerland experiences three to five debris-flow events per year, usually from May through October (Badoux et al., 2009). The catchment extends from the summit of the Illhorn mountain (2,716 m asl) to the fan apex at 850 m asl, after which the main channel drains into the Rhone River at 610 m asl (Hürlimann et al., 2003) (Figure 1). The slope failures that frequently occur on the steep lateral slopes (~40°) of the upper catchment provide the source sediment material for the initiation of the debris flows (Schlunegger et al., 2009). The debris fan volume (~500 × 10^6 m^3) is relatively large for the Alps, and the fan has an average slope angle of ~5.5° (Badoux et al., 2009).

A new force plate with an area of 8 m^2 (4 m extend perpendicular to the flow direction and 2 m extend in the flow direction), was installed in 2019 with a design similar to that described by McArdell et al. (2007). The concrete check dam upstream of the plate guides the flow onto the plate without any abrupt changes in channel topography, thereby ensuring that the forces measured are generated by the weight of the flow and the fluctuations produced by the boulders carried by the flow. Both the force plate and the concrete base of the check dam upstream of it are horizontal (McArdell et al., 2007). Vertical forces are the sum of four load cells situated underneath the corners of the force plate. Herein, the vertical force data (collected at either 2,400 or 9,600 Hz) are grouped into adjacent non-overlapping bins of 1 s duration, and both the maximum values and the median values of the normal forces are determined for each bin. The measured basal (non-fluctuating) forces and the basal fluctuating forces are the median forces and the lower quantile (25%) of the maximum-to-median force differences in each bin, respectively (see Text S1 and Figure S1 in Supporting Information S1).

Flow depth is determined from a laser sensor installed on the bridge above the force plate (Figure S3a in Supporting Information S1). The average frontal velocity of the flow is measured as the time of travel between a check dam 140 m upstream of the force plate and the force plate itself. To quantify the number and size of the cobbles and boulders (referred to as boulders hereafter) transported within the debris flows we measured the long (a-axis) and intermediate (b-axis) axes of each boulder passing over check dam (CD) 29 at the measurement station. We did this on subsequent movie frames with a time interval of 1 s, which may have rendered the passage of some boulders unnoticed but gives a good overall representation of the boulder size and quantity throughout the studied flows. The minimum b-axis of the boulders clearly visible on the movie frames is ~0.15–0.20 m, so only boulders exceeding these diameters have been measured. Furthermore, only boulders at the surface of the flow could be measured, and some boulders may be partly to completely shielded by larger boulders, inhibiting determination of their dimensions.

A seasonal campaign seismic network has been repeatedly installed around the Illgraben catchment to increase early warning capabilities (Chmiel et al., 2021, Figure 1). Except for station ILL11 operating with a Trillium compact sensor with a low frequency corner at 120 s, all stations are equipped with Lennartz-1s sensors with a flat response between 1 and 100 Hz. All stations have a sampling rate of 100 Hz. In this study, we analyze six well documented debris flows that occurred in 2019.

3. Model and Method

3.1. Sources of Debris-Flow Seismic Signals

While a diversity of potential sources of basal forces can generate seismic signals, only those forces that vary over relatively short time scales can generate high frequency seismic waves (Allstadt et al., 2020; Gimbert et al., 2014). We neglected the contributions of changes in the debris-flow bulk properties, such as the flow depth, weight, and density, although their exact role in seismogenesis is poorly understood. Instead, we expect that the high frequency seismic signals generated by debris flows originate from basal force fluctuations on shorter, sub-second time scales. This includes the random single-particle impacts (Farin et al., 2019) and force chain rearrangements (Campbell, 2006; Estep & Dufek, 2012). These source mechanisms are active at the same time (Campbell, 2006). Hence, at a given time t and over the area S_{bed} of the channel section, the typical magnitude of the basal force fluctuations ΔF_i^t is controlled by the random impact force $F_{T,i}^c$ caused by multi-particle force chains and the random single-particle impact force $F_{T,i}^p$, where i = V for vertical and H for the vector sum of two orthogonal horizontal directions.

3.1.1. Random Single-Particle Impact

In flows with a small solid volume fraction, a series of random individual particle impacts dominates force transmission, as proposed in the Tsai model (Farin et al., 2019, Figure 1d). For an instantaneous Hertzian contact (Hertz, 1882; Johnson, 1987), following Farin et al. (2019) we suppose the impulse I_i (in units of kN) transferred by an individual particle to be:

$$I_i = (1+\lambda) m u e_i \approx (1+\lambda) m w f_i \tag{1}$$

where λ is the basal coefficient of restitution (0 for a fully inelastic impact and 1 for a fully elastic impact), m is the particle mass (in units of kg), u is the impact velocity of particles with respect to the bed (in units of m/s), e_i is the unit impact vector ($e_V = \cos\psi$, $e_H = \sin\psi$, where ψ is the polar angle of impact with respect to the vertical), w is the flow velocity (in units of m/s), and f_i is a dimensionless function of the ratio between fluctuating velocity δw and w. Gimbert et al. (2019) observed the basal coefficient of restitution $\lambda \approx 0.13$ in flume experiments. Here, we assume $\lambda = 0.13$ for simplicity. For a spherical particle, $m = \pi \rho_s D^3/6$, where D is the particle diameter (in units of m) and ρ_s is particle density (~2,500 kg/m^3; Iverson, 1997). For a sampling frequency less than 100 Hz, a single particle impact at time $t = t'$ can be approximated as an instantaneously exerted force $F_{1,i}^p(t, D) = I_i \delta(t - t')$ (Tsai et al., 2012), where $\delta(t)$ is the Dirac delta function.

In the frequency domain the typical magnitude of the sum of individual fluctuating forces that occur randomly in time scales linearly with the square root of the total number of forces (e.g., Tsai et al., 2012). Thus, the total impact force $F_{T,i}^p$ (in units of kN) of the flow at a time t and over an area S_{bed} of the channel section (in units of

m^2), has a frequency spectrum, which has a magnitude proportional to the spectral magnitude (Farin et al., 2019; Tsai et al., 2012). Hence, the power spectral density (PSD) of the total impact forces $|\tilde{F}^p_{T,i}|^2$(in units of kN^2/Hz) can be expressed as:

$$\left|F_{\sim T,i}^{\ p}(f,t)\right|^2 = \int_D \left|\tilde{F}^p_{1,i}(f,t,D)\right|^2 R(D) S_{\text{bed}}\, d\, D \tag{2}$$

where $R d\, D$ represents the total impact rate, per unit surface area of the debris flow, of particles with diameters in $(D, D + \mathrm{d}D)$ and $\tilde{F}^p_{1,i}$ is the short-time Fourier transform of a single particle impact force $F^p_{1,i}$ over time window t_{win}. The integration over the distribution of particle size D can be removed if one determines an effective particle diameter D_e satisfying $D_e^x \approx \int_D D^x P(D) d\, D$, where x is the power of D in the relation between seismic power radiated per unit area of debris flow and D, and $P(D)$ is the particle size probability density.

3.1.2. Multi-Particle Force Chains

Inter-particle forces in flows with high particle concentrations often form force chains (Estep & Dufek, 2012). These force chains rapidly rearrange in dynamic granular systems due to further shearing, vibration, and particle collision, which cause locally extreme basal forces (Campbell, 2006; Estep & Dufek, 2012; Furbish et al., 2008; Majmudar & Behringer, 2005). We ignore the energy loss caused by the differences of particle sizes in the force chain and plastic deformation in the interaction between particles and muddy fluid. Force transmission via force chains is expected to be instantaneous and does not require stable chains for long periods of time (Estep & Dufek, 2012), and can be simply conceptualized as the correlated impacts of multiple particles.

For simplification, we assume that (i) the polar angles ψ of impact with respect to the vertical are constant in a force chain (Campbell, 2006; Thomas & Vriend, 2019), and (ii) the particle diameters D in a force chain are the same. We further assume that all force chains (iii) extend in a straight line from the channel bed to a given height (Campbell, 2006), and (iv) move as a block, implying that a force chain of N_1 particles has an effective mass of $N_1 m$ and transfers an impulse of magnitude $N_1 I_i$ to the bed during each impact. Assumptions (i) and (iii) agree with the simplified model of Campbell (2006) and assumption (i) is partially justified by the experimental results of Thomas and Vriend (2019). Assumption (ii) is reasonable when analyzing the effective particle diameter D_e. Assumption (iv) is not included in Campbell (2006), but equivalent results are obtained by supposing that each particle in the force chains impacts its lower neighbor at the same rate as the basal particle, with the entirety of the force transmitted directly to the bed. Furthermore, for assumption (iv), a force chain as a block, having a larger effective mass than an individual particle, will undergo impacts of longer duration. However, even if the mass of a force chain reaches the mass of a spherical particle with diameter similar to the flow depth h (which is always less than 2 m in the Illgraben torrent), the impact time can be expected to be instantaneous for a sampling frequency less than 100 Hz (Tsai et al., 2012).

Hence, at a given time window t_{win} and over an area S_{bed} of the debris flows, the random impact force spectral magnitude $|\tilde{F}^c_{T,i}|$ caused by multi-particle force chains can be expressed as:

$$|\tilde{F}^c_{T,i}(f,t)| = N_c |\tilde{F}^P_{T,i}(f,t)| \tag{3}$$

where N_c is the root-mean-squared (RMS) number of particles in the multi-particle force chains over the area S_{bed}. Note that for $N_c = 1$, implying the basal fluctuations are generated by random single-particle impacts, then $|\tilde{F}^c_{T,i}(f,t)| = |\tilde{F}^P_{T,i}(f,t)|$. This means that the random single-particle impact case can be treated as a special case of the multi-particle force chains where the particle's number in the force chains is 1. If N is regarded as the RMS number of particles over all impacts from multi-particle force chains and single particles at a time window t_{win} and over the area S_{bed}, the basal fluctuating force spectral magnitude $|\tilde{F}^t_i|$ can be expressed as:

$$|\tilde{F}^t_i(f,t)| = N |\tilde{F}^P_{T,i}(f,t)| \tag{4}$$

N can be expressed as: $N = (L_c/D)^\eta$, where L_c (in units of m) is the maximum length of force chains at a time window t_{win} and over the area S_{bed}, and η is a dimensionless parameter reflecting the relative contributions of random single-particle impact and of random impact caused by multi-particle force chains to the basal fluctuations, $0 \le \eta \le 1$. Note that both the single particles and the multi-particle force chains with length less than L_c can cause

$\eta < 1$. Furthermore, changes in both the number of particles in a force chain and the number of multi-particle force chains can change the relative contribution of the force chains to the basal fluctuation. For simplicity, we do not distinguish the changes in the relative contribution of multi-particle force chains caused by these two physical processes. To estimate L_c, we assume that the debris-flow particles interact with bed roughness of similar length scales l as the bed consists of deposits from previous flows so that $l = D$ (Farin et al., 2019). Accounting for the range of accessible angles given a bed of closely spaced particles with uniform size similar to that of the impacting particle, the impact angle with respect to the channel bed normal $\psi + \theta$ is in the range of 0–$\pi/6$ (Figure S3b in Supporting Information S1), and thus $L_c = h/\cos(\pi/6)$ (Figure 1).

3.1.3. Flow Velocity and Rate of Particle Impact

The calculation of the force spectral magnitude $|\tilde{F}_i^t|$ requires estimates of the flow velocity w and the rate of particle impact R. Here, for the thin flow case ($h \sim (1-10)D$), we assume that the vertical flow velocity profile can be approximated by a constant-velocity plug flow, even if $N > 1$. We simply use the depth-averaged flow velocity $\overline{w}$ (in units of m/s) to approximate w. $\overline{w}$ depends on flow rheology, which in turn depends on flow depth, bed slope, and material properties (water content, particle sizes, bed roughness; Johnson et al., 2012; Silbert et al., 2001). Simplified empirical formulas assume a non-linear relation between $\overline{w}$ and flow depth h (in units of m), which is generally expressed as (Hungr, 1995; Hungr et al., 1984; Rickenmann, 1999): $\overline{w} = \Lambda h^{\alpha}$, where α is an empirical constant, $\Lambda = C(\tan\theta)^{\beta}$ with the empirical constants C and β. α, β and C depend on the debris material characteristics, such as the flow-resistance coefficients, lumped coefficient, and dynamic viscosity and density of the grain-water mixture.

There are about $4\bar{\phi}P(D)/(\pi D^2)$ particles per meter square of the bed, where $P(D)\mathrm{d}D$ is the probability that the particle size lies between D and $D + \mathrm{d}D$, and $\bar{\phi}$ is the average solid volume fraction. The solid volume fraction in debris flows generally ranges from 0.4 to 0.8 (Iverson, 1997). For simplicity, $\bar{\phi}$ is assumed to be 0.6. The velocity fluctuation δw departing from the steady state flow (Farin et al., 2019) causes the particle impacts. Hence, the rate of random particle impacts per unit surface area of the bed, per unit particle diameter, is expected to be $R \approx \delta w\bar{\phi}P(D)/(lD^2) = \delta w\bar{\phi}P(D)/D^3$. For the thin flow case, most clasts impacting roughness elements of the channel bed will significantly disturb $\overline{w}$, forcing the velocity to depart from the average flow speed, and thus imply that the fluctuating velocity scales with the flow velocity $\delta w \sim \overline{w}$ (Farin et al., 2019). Hence, the rate of particle impacts can be expressed as: $R \approx \overline{w}\bar{\phi}P(D)/D^3$.

3.2. Basal Force Fluctuation

Using Equations 1, 2 and 4, the impact rate R and the depth-averaged flow velocity $\overline{w}$, we can now express the spectral magnitude $|\tilde{F}_i^t|$ of the theoretical basal fluctuating force at a time window t_{win} and over an area S_{bed} of the channel section:

$$|\tilde{F}_i^t(f,t)| \approx \frac{\pi(1+\lambda)\rho_s\Lambda^{1.5}\sqrt{\bar{\phi}S_{\mathrm{bed}}}}{6(\cos\frac{\pi}{6})^{\eta}} {D_e}^{1.5-\eta}h^{1.5\alpha+\eta}f_i \tag{5}$$

where f_i is a dimensionless function of the ratio between δw and $\overline{w}$, as specified by Farin et al. (2019), and can be expressed as: $f_V \approx f_z\cos\ \theta - f_x\sin\ \theta$, $f_H = \sqrt{f_{H'}^2 + f_y^2} \approx \sqrt{(f_z\sin\ \theta + f_x\cos\ \theta)^2 + f_y^2}$, where the subscripts x, y, and z represent the downslope, transverse, and normal directions respectively, and H′ represents the projection of horizontal direction H on the x–z plane. For thin flow, we can simplify and assume $\delta w \sim \overline{w}$, and thus f_x, f_y, and f_z are 0.17, 0.15, and 0.59, respectively (Farin et al., 2019). To verify the theoretically predicted basal fluctuations against the force plate data, the basal fluctuating force spectrum in the frequency domain needs to be converted into the basal fluctuating force in the time domain. Here, we calculate the RMS basal fluctuating force for each t_{win}, and treat it as the typical magnitude of theoretical basal fluctuating forces ΔF_i^t. According to Parseval's theorem, the ΔF_i^t (in units of kN) in the time domain for each t_{win} can be expressed as (Text S2 in Supporting Information S1):

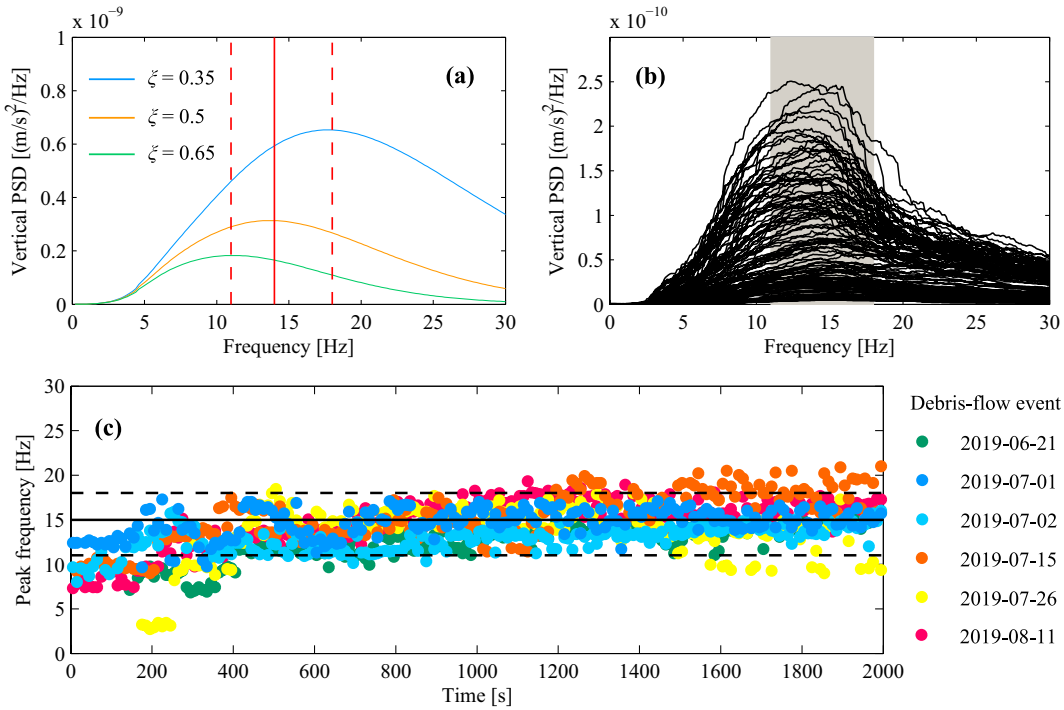

Figure 2. Peak frequency of power spectral density (PSD) of seismic signals. (a) The theoretical PSD calculated with different scattering damping ratios of soil ξ. (b) The PSD of measured seismic signals of 10 s time windows, generated by the August 11, 2019 debris flow. (c) The peak frequency of PSD within individual time windows for each event. The black solid line is the peak frequency (14 Hz) corresponding to when ξ is 0.5. The black dotted lines represent a ξ uncertainty of 30% corresponding to a peak frequency range between 11 and 18 Hz.

$$\Delta F_i^t(t) = \sqrt{\frac{K}{M t_{\text{win}}} \sum_{m=0}^{M-1} |\tilde{F}_i^t(f_m, t)|^2} \tag{6}$$

where M is the number of samples in the fast Fourier transform, f_m is the frequency at sample m, and K is the number of samples in t_{win}. Here, we choose time windows of 1 s, and assume that the basal fluctuating force spectrum is constant over the frequency range of 1–30 Hz, and thus $1/M \sum_{m=0}^{M-1} |\tilde{F}_i^t(f_m, t)|^2 = |\tilde{F}_i^t(f_0, t)|^2$. Furthermore, because sampling rates of the parameters on the right side of Equation 4 are around 1 Hz, $\Delta F_i^t(t) = |\tilde{F}_i^t(f_m, t)|$.

3.3. Seismic Wave Propagation

To model high frequency seismic signals generated by debris flows, we begin with the theoretical model of Zhang et al. (2021) for the PSD of debris-flow seismic signals (see Text S3 in Supporting Information S1). We assume that the signals recorded at a given seismic station are controlled by the debris flows flowing through a channel section with unknown area S_{bed}, that the contribution of force fluctuations applied outside S_{bed} can be neglected, and that force fluctuations applied inside S_{bed} can be approximated as being concentrated at a single point.

We represent the source-station distance r by the shortest distance from the channel to the recording seismic station. For station ILL11, the value of r is 15 m. The basal fluctuation is assumed to be composed of delta functions so that its PSD is independent of frequency. When the peak frequency is measured for a known r, the value of the soil's scattering damping ratio ξ can be estimated to reproduce the measured peak frequency (Zhang et al., 2021). We then obtain a value of the soil's scattering damping ratio ξ of 0.5 for station ILL11, corresponding to the peak frequency of 14 Hz (Figure 2a). For a given station, r and ξ are constant. However, the peak frequency of seismic signals is not stationary due to the sediment deposition and erosion during run out, which causes uncertainties in the value of ξ. In order to account for scour/fill between events in the seismic ground model, we calculate a ξ

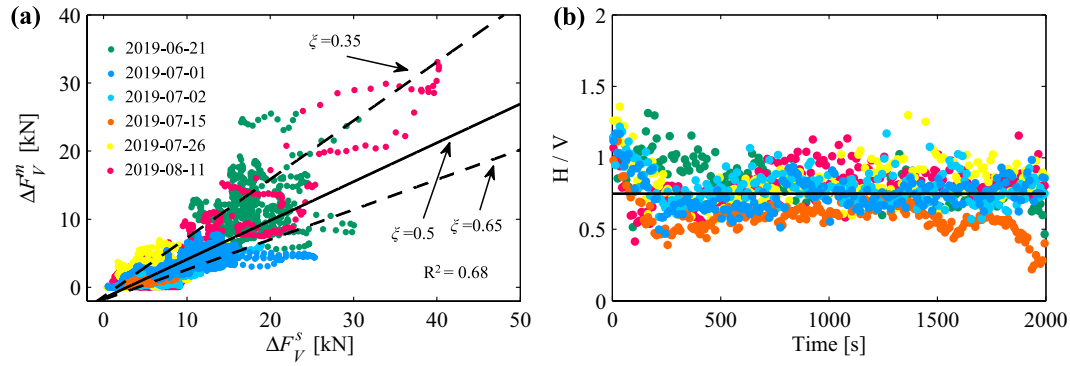

Figure 3. Basal fluctuating forces. (a) Basal vertical fluctuating forces measured at the force plate ΔF_V^m versus root-mean-squared (RMS) seismically derived basal fluctuating forces ΔF_V^s. The solid line represents the linear fit between ΔF_V^m and ΔF_V^s for $\xi = 0.5$. Dashed lines represent the linear fit between ΔF_V^m and ΔF_V^s for $\xi = 0.35$ and 0.65. (b) Ratio of the horizontal to vertical RMS seismically derived basal fluctuating forces horizontal-to-vertical force fluctuations ratio (HVR). The black line represents the average HVR of all events (~0.75).

uncertainty of 30%, corresponding to a peak frequency range between 11 and 18 Hz that contains most frequency peaks (Figures 2b and 2c).

4. Results

4.1. Seismically Derived Basal Force Fluctuation

For all events, we calculate the PSDs for signals within time windows of 10 s. All PSDs are smoothed with a 5 Hz running average. Using damped least squares inversion and the PSD of seismic signals between 1 and 30 Hz in individual time windows (Zhang et al., 2021), we obtain the spectral magnitude $|\tilde{F}_i^s|$ of the seismically derived basal fluctuating force for each time window of 10 s (Text S3 in Supporting Information S1), and assume that it is a constant over the frequency range of 1–30 Hz. We calculate the RMS seismically derived basal fluctuating force ΔF_i^s for each time window with Equation 6, and treat it as the typical magnitude of seismically derived basal fluctuating force for each time window.

To compare with the measured data (i.e., the flow depth and the weight), we then resample ΔF_i^s to 1 Hz using an anti-aliasing FIR filter with a Kaiser window. Note that station ILL11 is located 140 m upstream of the force plate. Because there are no video data at this position, it is difficult to accurately estimate the time when the flow front arrives at the seismic source section with area S_{bed}. Hence, we manually align the inverted force with the measured data recorded at the force plate to ensure the best match between the two. Furthermore, we ignore sediment deposition and/or erosion of debris in the 140 m channel section between station ILL11 and the force plate.

For unknown reasons, there exist outliers in the force plate and flow depth data. For example, the maximum ΔF_V^m of the June 21 event is about 6.9×10^{13} kN, which is far greater than the expected range of ΔF_V^m. If the $\Delta F_V^m(t)$ is greater than $100 \times F_V^m(t)$, it is treated as an outlier. Furthermore, if the flow weight does not change significantly during run-out, the corresponding flow depth will generally not change significantly. If the flow depth $h(t)$ is greater than $F_V^m(t)/g\rho_w S_{\text{bed}}$, where ρ_w is the water density (ρ_w =1,000 kg/m^3), the $h(t)$ is treated as an outlier. These outliers in h and ΔF_V^m account for only a small fraction of the measured data (Figures S4 and S5 in Supporting Information S1), and are ignored in the following analysis.

Due to the difference in the area of S_{bed} and of the force plate S_{plate} and the simplification in the seismic ground model, we cannot directly compare the absolute magnitude of the seismically determined basal force fluctuation with the force plate. However, as expected, there exists a scale relation between the RMS seismically derived basal fluctuating force ΔF_V^s and the measured basal vertical force fluctuations ΔF_V^m (Figure 3a). The linear fit between the ΔF_V^m and the ΔF_V^s corresponding to the ξ uncertainty of 30% contains about 75% of ΔF_V^m measurements. Using the scale correlation between $\Delta F_V^s(\xi = 0.5)$ and ΔF_V^m, we scale ΔF_V^s to obtain a corrected seismically derived basal force fluctuation $\Delta F_V^{s'}$. As expected $\Delta F_V^{s'}$ correlates with ΔF_V^m over the full extent of individual flows (Figure 4), which validates the seismically derived basal fluctuating forces.

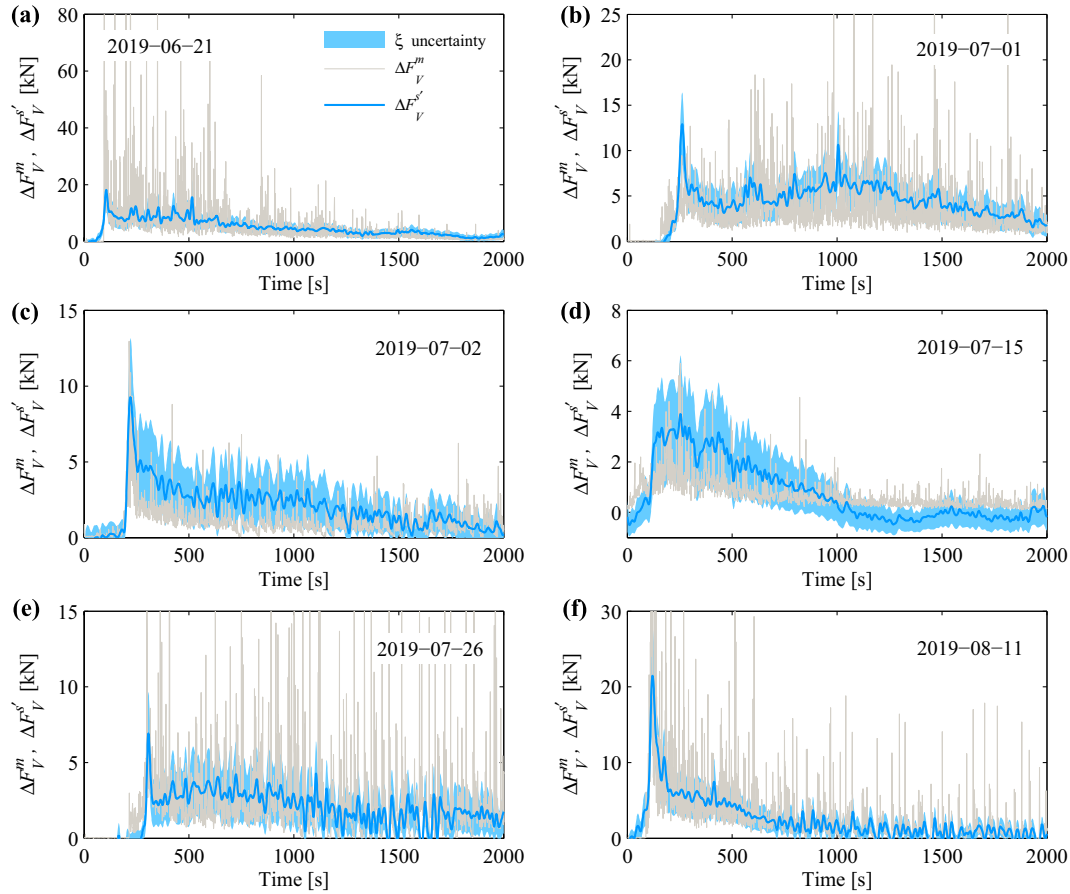

Figure 4. Measured basal vertical force fluctuations ΔF_V^m (gray lines) at the force plate and corrected seismically derived basal vertical force fluctuation $\Delta F_V^{s'}$ (blue lines).

For each event, the seismically derived horizontal-to-vertical force fluctuations ratio (HVR) is nearly constant during the passage of the debris flows past the seismic station. The HVR is close to a constant 0.75 for all events. Nevertheless, there exist some deviations in the average HVR within and between events. For example, the July 15, 2019 event consistently shows the lowest HVR.

4.2. Correlations Between Basal Force Fluctuations and Bulk Flow Characteristics

We observe that the measured basal (non-fluctuating) vertical forces F_V^m correlate with the envelope of the measured basal fluctuating forces ΔF_V^m, except for the flow front (Figures 5b and S6b-S10b in Supporting Information S1). Therefore, there exists a relationship between the ΔF_V^m and the F_V^m at a force plate (Figure 6b). We tested both linear and power law fits to the relation between ΔF_V^m and F_V^m. The non-linear relation can better explain the relation between the ΔF_V^m and the F_V^m ($R^2 = 0.80$ for the power-law fit, $R^2 = 0.67$ for the linear fit; Figure 6b and Table 1). The seismically derived basal fluctuating forces ΔF_V^s are nonzero before the flow front reaches the seismic station because station ILL11 records the seismic signals generated by the approaching flow front. Similar to the weight F_V^m, there is a relationship between ΔF_V^m and the flow depth h (Figure 5d). For individual events, the temporal variation of ΔF_V^m correlates with that of h, except for the flow front (Figures 5d and S6c-S10c in Supporting Information S1). A non-linear relation better explains the relation between ΔF_V^m and h (Figure 6a). We then separate data from different events and fit a power law to the relation between ΔF_V^m and h for each event (Figure 7 and Table S1 in Supporting Information S1). We observe that the flow depth dependence of basal force fluctuations varies between events, which in the context of our model implies that the relative contributions of single-particle random impacts and of random impacts caused by multi-particle force chains on the basal force fluctuations is different in each event. Furthermore, we find that there is a negative correlation between h and

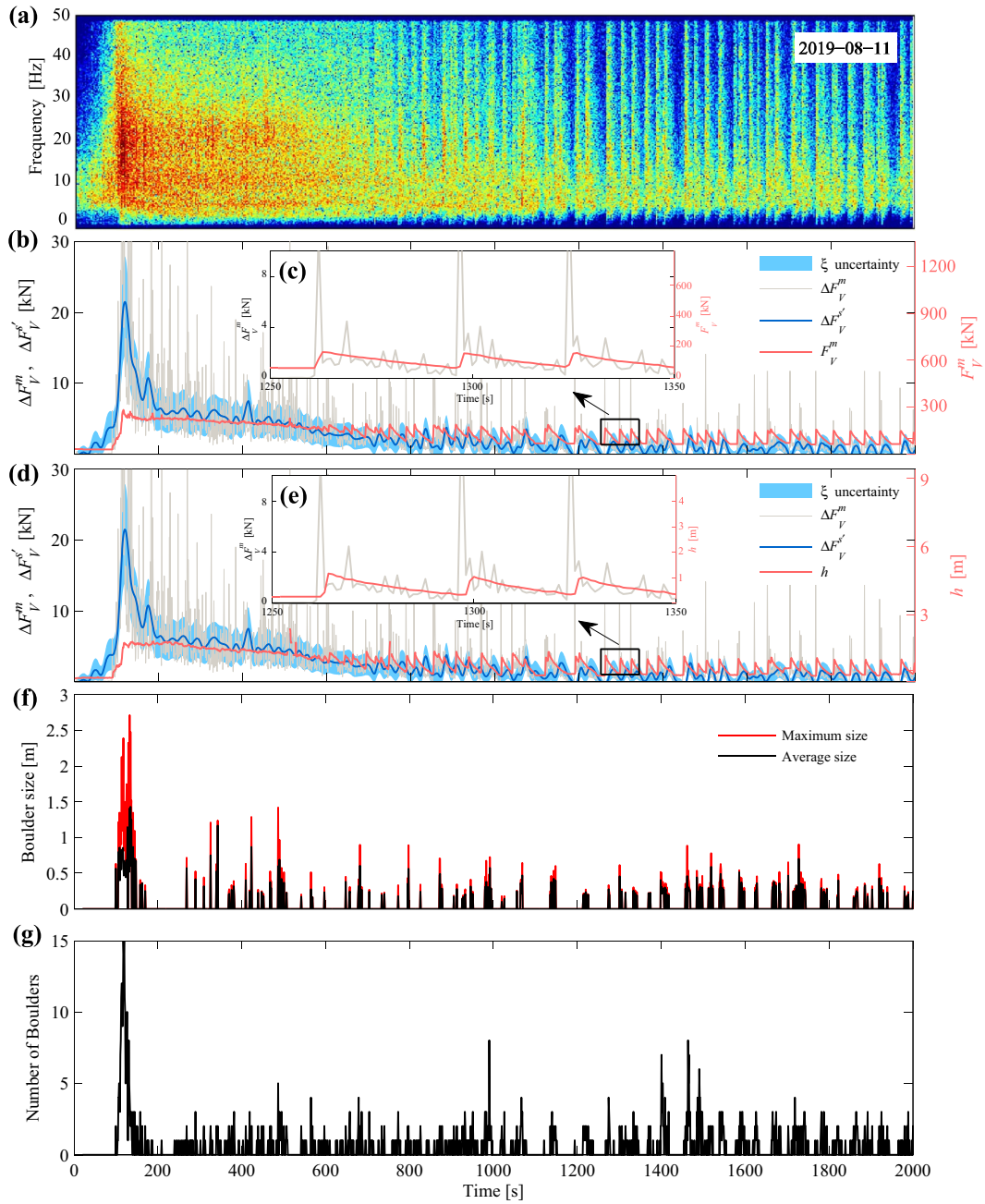

Figure 5. Measurements at CD 29 and seismically inverted results from the August 11, 2019 debris flow. (a) Spectrogram of vertical seismic signal recorded at the station ILL11. (b and c) Corrected seismically derived vertical basal fluctuating forces $\Delta F_V^{s'}$, measured vertical basal fluctuating forces ΔF_V^m and basal (non-fluctuating) forces (weight) F_V^m recorded at the force plate. Panel (d and e) $\Delta F_V^{s'}$, ΔF_V^m and flow depth h. (f and g) Size and number of boulders from video recordings. The average size denoted by the black line in panel f corresponds to the mean b-axis of all the measured boulders (number displayed in panel g) at each point in time.

the bulk density ρ expressed as $\rho = F_V^m / ghS_{\text{bed}}$ (Figure 6d). This may be one of the reasons why the power of F_V^m (2.35) in the non-linear relation between the ΔF_V^m and F_V^m is larger than the power of h (1.69) in the non-linear relation between the ΔF_V^m and h because ρ only affects the latter relation. An interesting phenomenon is that the bulk flow characteristics (F_V^m and h) always slightly lag behind ΔF_V^m in the roll-wave-like surges in the debris-flow tail (Figures 5c and 5e). This may be another manifestation of the conveyer-belt mechanism that usually concentrates large particles near the flow front (Pierson, 1986) and in this case traps coarse grains in front of roll wave

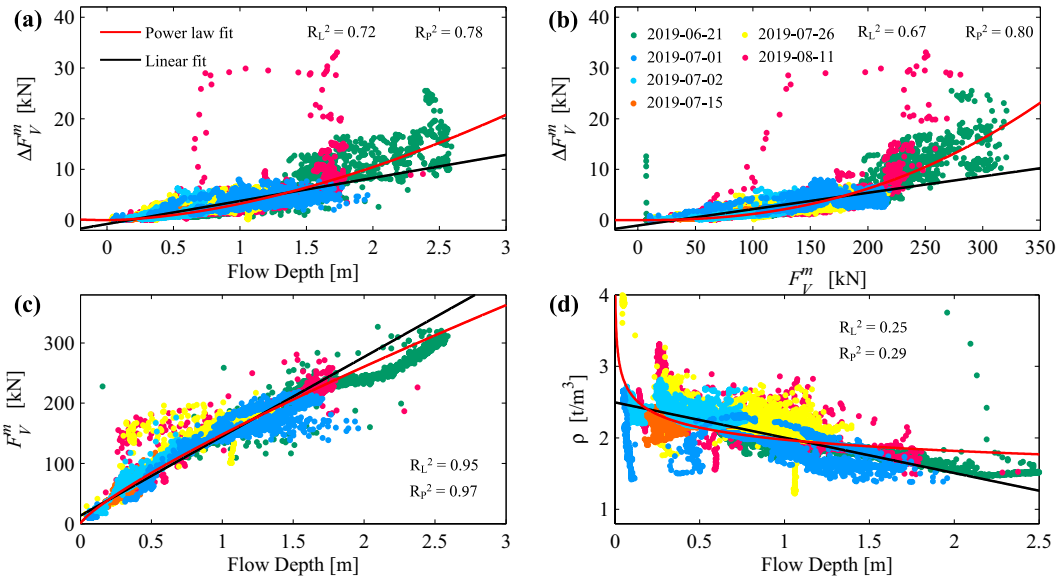

Figure 6. Measured basal fluctuating forces and the bulk flow characteristics. (a and b) Measured basal fluctuating forces ΔF_V^m versus the flow depth h and the measured basal forces F_V^m, respectively. (c) F_V^m versus the flow depth. (d) Bulk density ρ versus the flow depth. The red and black lines are the power and linear law fits, respectively. R^2 is goodness of fit, subscripts L and P denote linear and power law fits, respectively. ΔF_V^m and ρ are smoothed with a 20 s running average. Outliers in h and ΔF_V^m are ignored.

surges. Alternatively, evenly distributed coarse particles in the flow tail are transiently compressed as roll wave surges pass (Viroulet et al., 2018).

For the flow front, the basal fluctuating forces ΔF_V^m measured at the force plate and the seismically inverted basal fluctuating forces ΔF_V^s exhibit distinct peaks (Figures 5 and S6-S10 in Supporting Information S1) while the measured basal (non-fluctuating) vertical forces at the force plate F_V^m and the flow depth h do not. The differences between the bulk flow characteristics and the basal force fluctuations in the flow front may be due to the concentrations of large particles at the front (Figures 5f and 5g) that are transported to the flow front due to size segregation (Johnson et al., 2012). These large particles have larger impact forces on the bed and generate strong seismic signals (Figure 5a). However, only some of these peaks correspond to the observed passage of large boulders (such as the June 21, 2019 debris flow; Figure S6 in Supporting Information S1). This discrepancy may well be the result of the limitations in the boulder size measurement described earlier. Depending on other factors such as the concentration of particles in the flow, it is also possible that some of the largest particles, when transported above a matrix of smaller-size particles (such as upstream of the flow front), may be effectively carried in suspension in the flow and may not always generate force chain interactions with the bed.

Table 1
Linear and Power-Law Fits Between Various Flow Characteristics

		Linear fit: y = ax + b			Power law fit: y = mx^n		
y	X	A	B	R^2	m	n	R^2
ΔF_V^m (kN)	h (m)	4.54	−0.76	0.72	3.24	1.69	0.78
ΔF_V^m (kN)	F_V^m (kN)	0.03	−1.06	0.67	2.4×10^{-5}	2.35	0.80
F_V^m (kN)	h (m)	131.80	13.21	0.95	148.00	0.82	0.97
ρ (t/m^3)[a]	h (m)	−0.49	2.50	0.25	1.97	−0.12	0.29

Note. ΔF_V^m and F_V^m are the measured vertical basal fluctuating force and basal (non-fluctuating) force (weight) recorded at a force plate, respectively. h is the flow depth. ρ is the debris-flow bulk density.
[a]t represents metric tons.

4.3. Theoretical Basal Force Fluctuation

Using the measured data in the Illgraben torrent, we obtain an empirical relation between the depth-averaged downslope velocity $\bar{w}$ and the flow depth h expressed as $\bar{w} = 3.57h^{0.81}$ (see Text S4 and Figure S2 in Supporting Information S1). The force plate is horizontal (i.e., $\theta = 0°$). Based on Equations 5 and 6 and the empirical relation between h and $\bar{w}$, the typical magnitude of the theoretical basal fluctuating forces over a force plate with area of 8 m^2 for each time window of 1 s can be expressed as:

$$\Delta F_i^t(t, \eta, D_e) \approx 21.8 f_i (\cos\frac{\pi}{6})^{-\eta} D_e^{1.5-\eta} h^{1.22+\eta} \quad (7)$$

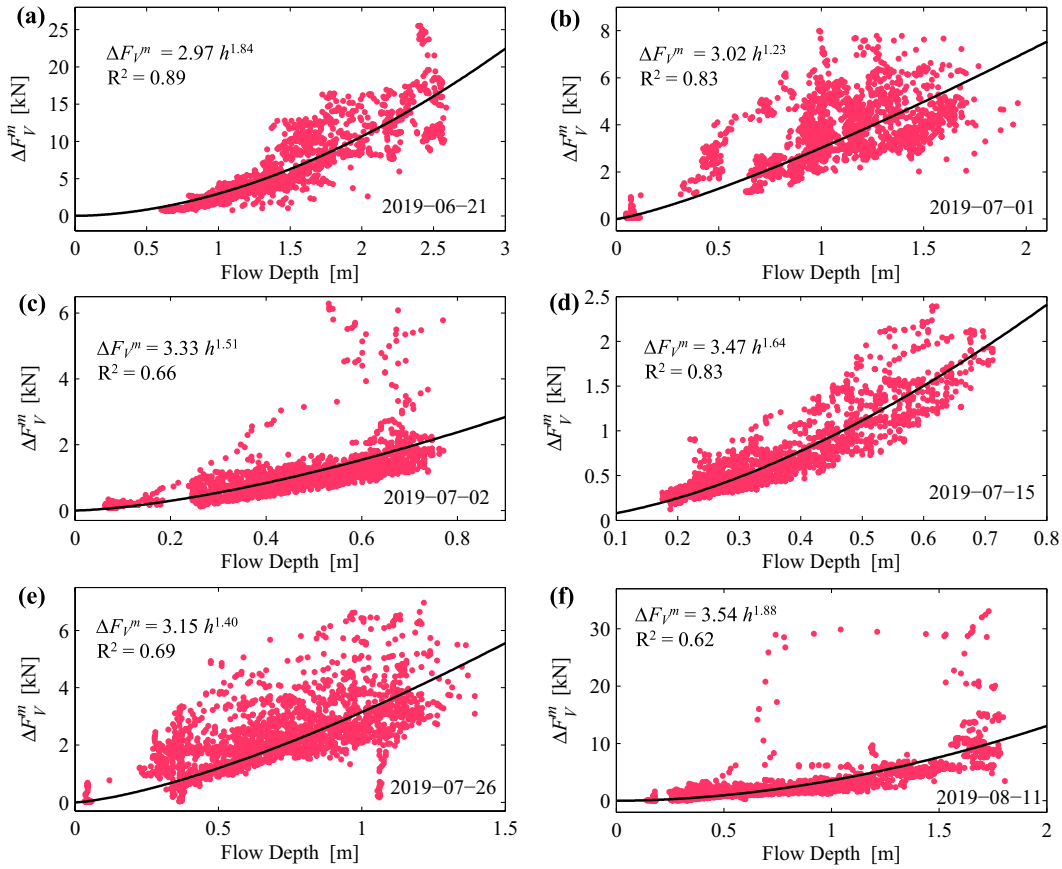

Figure 7. Measured basal force fluctuation ΔF_V^m versus flow depth. Black lines indicate power law fits. Outliers in h and ΔF_V^m are ignored.

where $f_V \approx 0.59\cos 0 - 0.17\sin 0 = 0.59$ and $f_H \approx \sqrt{(0.59\sin 0 + 0.17\cos 0)^2 + 0.15^2} = 0.23$. The particle size distributions in torrents are rarely available (e.g., Rickenmann et al., 2012) and the effective particle diameter D_e is therefore difficult to estimate. Here, we take the average boulder sizes estimated from the video recordings to be the effective diameter D_e.

When the dimensionless parameter η is 0 (i.e., $N = 1$), $\Delta F_i^t = 21.8 f_i {D_e}^{1.5} h^{1.22}$, which means that all impacts on the force plate result from single particles, the mechanism causing basal force fluctuations is the same as in the "thin-flow" model with $\delta w \sim \bar{w}$ of Farin et al. (2019). The difference between this "thin-flow" model and $\Delta F_V^t(\eta = 0)$ is that we use an empirical relation between flow velocity and flow depth to estimate depth-averaged flow velocities and hence representative particle impact velocities and the relation between basal force fluctuations and flow depth. We also used the "thin-flow" model to predict the basal force fluctuations (see Text S5 in Supporting Information S1). We observe that, except for July 15 and 26 events, $\Delta F_V^t(\eta = 0)$ is similar to the predictions of the "thin-flow" model of Farin et al. (2019) (including amplitude and shape; Figure 8), which provides support for our empirical relation between flow velocity and flow depth. One reason for the prediction discrepancies between these two events may come from the limitation of flow-velocity estimation.

When the value of η is 1, $\Delta F_i^t = 25.2 f_i {D_e}^{0.5} h^{2.22}$, which implies that all basal fluctuating forces are transmitted to the force plate via force chains extending from the surface of the flow to the base. We observe that the value of $\Delta F_V^t(\eta = 1)$ is always greater than that of $\Delta F_V^t(\eta = 0)$ in the flow front, while the differences between the two gradually decrease in the flow tail (Figure 8). As both flow depth and coarse particles decrease in the flow tail, both number of contacts in a force chain and number of force chains decrease, and the force transmission via a force chain to the force plate is closer to the individual particle random impact force. Furthermore, we observe that there are some limitations in predicting the basal force fluctuations using the random force caused by multi-particle force chains or the random single-particle impact force, separately. For example, the measured

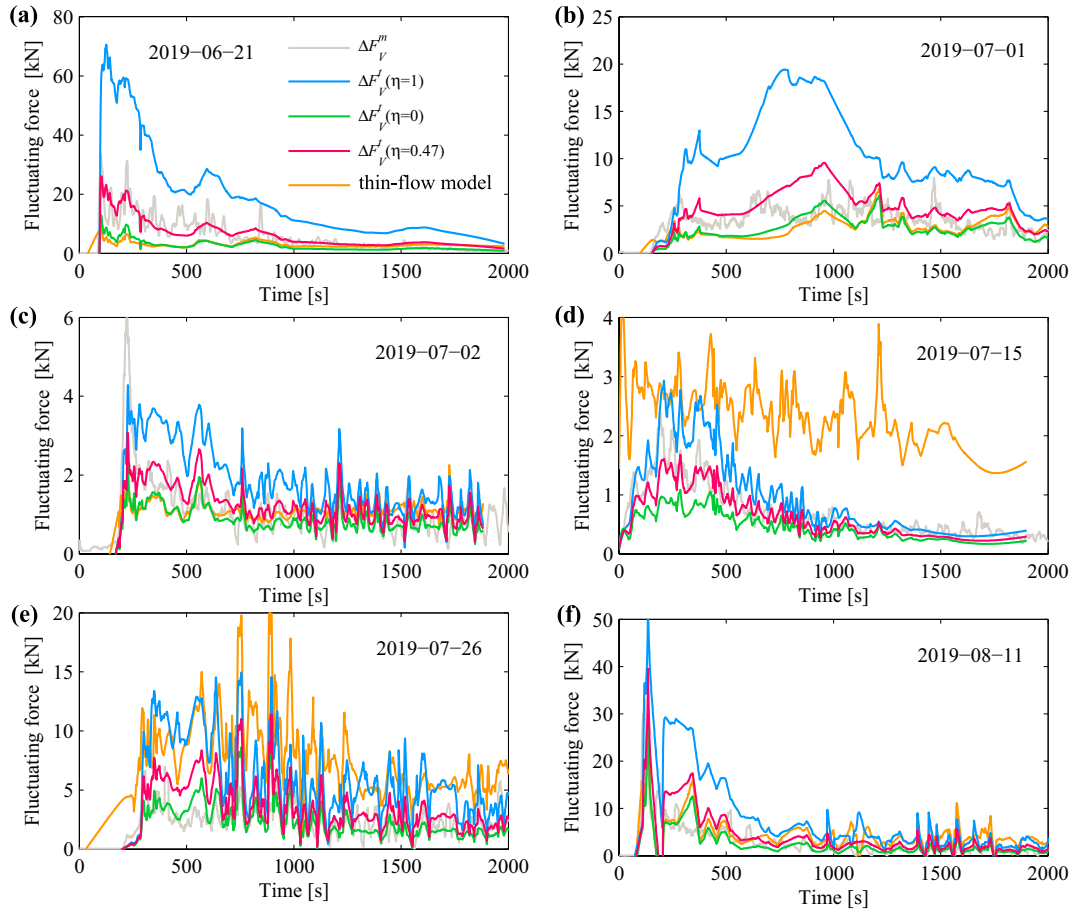

Figure 8. Measured basal force fluctuations ΔF_V^m at a force plate (gray lines) versus theoretical basal force fluctuations ΔF_V^t. The blue, green, and red lines represent the basal force fluctuation predictions with the value of η equal to 0, 1, and 0.47, respectively. The yellow lines are the basal force fluctuation predictions from the "thin-flow" model of Farin et al. (2019) (see Text S5 in Supporting Information S1). All theoretical basal force fluctuations are smoothed with a 10 s running average.

basal force fluctuations are always in between the theoretical predications for random single-particle impacts ($\Delta F_V^t(\eta = 0)$) and those for impacts of multi-particle force chains ($\Delta F_V^t(\eta = 1)$). Because the power of flow depth in the relation between the measured basal force fluctuations and the flow depth is 1.69 (i.e., $\eta = 0.47$; Figure 6), we take $\eta = 0.47$ and recalculate ΔF_V^t. As expected, we observe that $\Delta F_V^t(\eta = 0.47)$ can better predict the basal force fluctuations (Figure 8). Furthermore, we observe that although, by themselves, neither impacts of single particles nor impacts of multi-particle force chains can predict the basal force fluctuations for most events, the basal force fluctuations are closer to the multi-particle force chain prediction in the flow front of the July 15 event, and the basal force fluctuations are closer to the random single-particle impact prediction in the flow front of the July 26 event. Our model thus suggests that the basal force fluctuations are controlled by the random single-particle impacts and the random impacts caused by multi-particle force chains, and the relative contributions of these two physical mechanisms on the basal force fluctuations varies for different events and flow positions.

5. Discussion

In this study we examined high frequency force fluctuations at the base of debris flows and compared measurements with theoretical predictions based on a new model incorporating impact forces both from individual particles and from multi-particles force chains. We find that the measured basal force fluctuations at a force plate can be better predicted when both types of impact are considered at the same time.

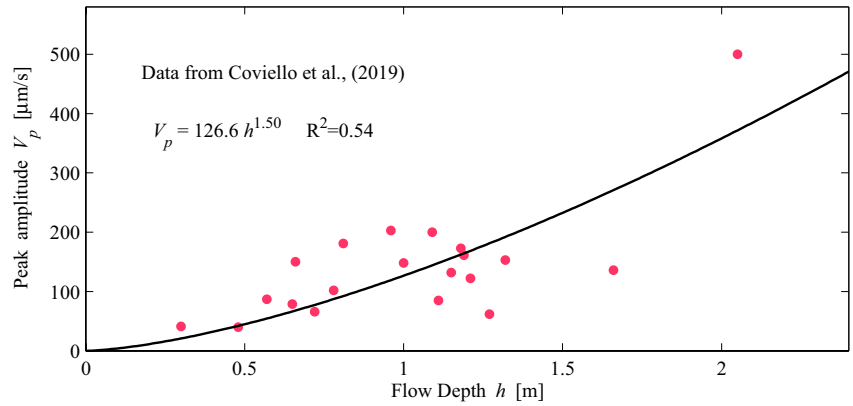

Figure 9. Peak amplitude of vertical seismic velocity generated by flow surges versus the flow depth of the surges, for debris flows in the Gadria basin (eastern Italian Alps) (see Coviello et al., 2019).

5.1. Relation of Basal Force Fluctuations to Flow Characteristics

With the basal force fluctuation model, we are able to explain the relation between the high frequency seismic signals and the other bulk properties, such as the bulk kinetic energy per unit bed area E_k and the momentum per unit bed area M_a. Based on the simplified fitting relation between the depth-averaged downslope flow velocity $\overline{w}$ and the flow depth, E_k and M_a can be expressed as: $E_k \sim 0.5\rho h\overline{w}^2 \sim 6.369\rho h^{2.61}$, and $M_a = \rho h\overline{w} \sim 3.569\rho h^{1.81}$. Assuming that the flow bulk density ρ remains constant, the bulk kinetic energy per unit bed area E_k and momentum per unit bed area M_a are controlled by the flow depth. In our model the flow depth dependence of basal force fluctuations has an exponent between 1.22 and 2.22, and a larger η value corresponds to the larger flow depth dependence. Furthermore, because the amplitudes of high frequency seismic signals are nearly proportional to the basal fluctuating forces (Allstadt et al., 2020), there exists a non-linear relation between the high frequency signal amplitudes and the flow depth, with exponent between 1.22 and 2.22. This is expected to explain the findings of Hibert et al., (2017), who found a roughly linear relation between high frequency signal amplitudes ($\sim h^{1.22} - h^{2.22}$) and momenta of large landslides M_a ($\sim h^{1.81}$). In addition, although the flow depth exponent (2.61) in the relation between E_k and flow depth exceeds the flow depth dependence range of high frequency signal amplitudes, there exists a theoretically non-linear relation between E_k and the flow depth. This relation is close to the findings of Coviello et al. (2019), who found a roughly linear relation between the bulk kinetic energy E_k ($\sim h^{2.61}$) and the peak amplitude of seismic vibrations.

5.2. Basal Force Fluctuation Model

5.2.1. Relative Contributions of Single Particles and of Multi-Particle Force Chains

For each debris-flow event in the Illgraben torrent, we calculate the best-fit relations $\Delta F_V^m = mh^n$ between different events' flow depths and measured vertical basal force fluctuations (Figure 7 and Table S1 in Supporting Information S1). We observe that the best-fit exponents n are different for different events (with non-overlapping 95% confidence intervals), but are in the range 1.22–2.22 predicted by our model. Similarly, measurements of Coviello et al. (2019) in the Gadria basin (eastern Italian Alps) show that the power of h in the best-fit relation between the peak amplitude of seismic signal (which is proportional to the typical magnitude of basal force fluctuations) and the flow depth is in the predicted range (1.22–2.22; Figure 9). Besides natural events, Allstadt et al. (2020) observed the best-fit flow depth dependence $\Delta F_V^m \sim h^{2.04}$ in two large-scale flume experiments, which is in the flow depth dependency range predicted by our model. These findings imply that according to our model, both random single-particle impacts and random impacts caused by multi-particle force chains are active during run out (e.g., Campbell, 2006).

The flow depth dependence of basal force fluctuations varies among events, which according to our model implies that the relative contributions of multi-particle force chains and of single particles to basal force fluctuations differ between events. The change in the relative contribution of multi-particle force chains is controlled by the changes in the number of particles in a force chain and/or the number of multi-particle force chains. However,

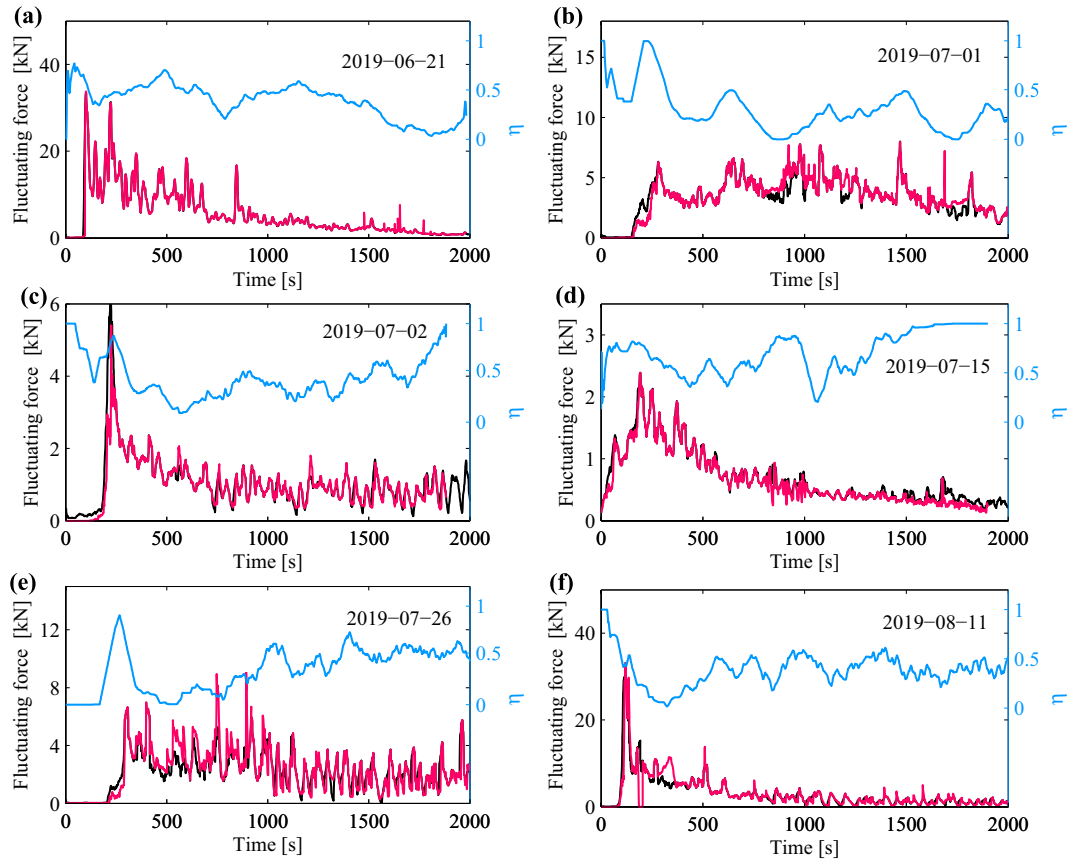

Figure 10. Basal fluctuation forces and best-fit dimensionless parameter η (blue lines). The black lines are measured basal force fluctuations ΔF_V^m at a force plate. The red lines are the basal fluctuations simulated by Equation 7 that best match the ΔF_V^m. The best-fit η is smoothed with a 100 s running average.

based on our measurements, it is challenging to distinguish between these two factors. We can only expect that in flows with large solid volume fraction, force chains are longer and/or more likely to form, and so are the dominant cause of basal force fluctuations. For example, in Allstadt et al. (2020)'s flume experiments with nearly saturated sediments, the best-fit exponent connecting flow depth to basal force fluctuations (2.04) is closer to the exponent that our model predicts when all impacts are of force chains extending from the flow's base to its surface (2.22) than to the exponent predicted when all impacts are of single particles (1.22). In natural events, however, a flow's solid volume fraction is rarely known.

In order to better simulate the measured basal vertical force fluctuations ΔF_V^m at a force plate, the dimensionless parameter η is treated as an empirical fitting variable that is time dependent and reflects the flow depth dependence of basal force fluctuations. Because the length of a representative force chain should be between the particle size D and the maximum force chain length L_c, η is expected to be in the range of 0–1. Here, we calculate the theoretical basal vertical force fluctuations ΔF_V^t using different η values, and then obtain the ΔF_V^t with the smallest disagreement to ΔF_V^m and the corresponding best-fit η value (Figure 10). As expected, we observe that the best-fit η value can be used to accurately predict the ΔF_V^m, and is consistent with the force chain length being in the physically expected range. Furthermore, possibly due to the fluctuation of local solid volume fractions in a flow, the best-fit η value varies significantly even within an event (Figure 10).

5.2.2. Practical Considerations

Our model shows that basal force fluctuations (which are proportional to the high frequency seismic signals) are strongly controlled by particle size and flow depth, which has also been shown experimentally (de Haas et al., 2021). It is difficult to measure the particle size distributions in torrents. Using the video data to estimate the particle size has unavoidable limitations and uncertainties, which is one of the reasons for the differences

between simulated and measured basal force fluctuations. Furthermore, de Haas et al. (2021) found that representative particle diameters D_e cannot be accurately estimated even in small-scale experiments. According to our model, D_e satisfies $D_e^{1.5-\eta} \approx \int_D D^{1.5-\eta} P(D) d\,D$, so it will vary within a flow according to changes in η or in the local particle size distribution. Here, for simplicity, we use the average boulder size from the video data as the effective particle size. This average boulder size is likely larger than the 73rd percentile D_{73} of particle size distribution, which is the effective particle size derived by Farin et al. (2019) for the "thin-flow" model, and perhaps closer to D_{94} predicted by Tsai et al. (2012). With our data, we cannot say which percentile most closely resembles the effective particle size. Furthermore, for a given flow height, the force chain prediction has a weaker particle size dependence ($D_e^{1.5-\eta}$) than that of the impact force prediction ($D_e^{1.5}$; Tsai et al., 2012; Zhang et al., 2021).

There are uncertainties in the local solid volume fraction, influencing the amplitude of ΔF_V^t. For the solid volume fraction, the ΔF_V^t are proportional to the square root of the average solid volume fraction $\bar{\phi}$. In addition, the expected range (0.4–0.8) of the solid volume fraction is not large (Iverson, 1997), so the changes in $\bar{\phi}$ cannot significantly influence the amplitude of ΔF_V^t. However, it is meaningless to analyze only the influence of the change of $\bar{\phi}$ on ΔF_V^t, because the influence of $\bar{\phi}$ on the ΔF_V^t manifests itself via the number and length of the force chains. In flows with larger local solid volume fractions, the particles are expected to more readily form force chains which dominate the basal force fluctuations. However, based on our data set, we cannot analyze the relation between the solid volume fraction and the particle numbers in a force chain and/or the number of force chains.

Another source of uncertainty is the basal coefficient of restitution λ, which will affect the amplitude of ΔF_V^t. Although some dedicated experiments (e.g., Durda et al., 2011; Jackson et al., 2010) found λ to be ≈ 0.6, greater than the value of Gimbert et al. (2019) for similar materials (steel and rocks), we still choose the value ($\sim$0.13) from the Gimbert et al. (2019) flume experiments. This is because the concerns of Gimbert et al. (2019) on both the inelasticity of the mechanical response and the extra impact energy loss caused by the geometrical effect of the particles, may exist in our theory and measurement background. Similar to the concerns of Gimbert et al. (2019), particles contact each other in force chains with their center of mass not being perfectly aligned, generating extra impact energy loss with respect to aligned particles. Furthermore, the loose sediment (clay and small sized particles) carried by the debris flows will reside between the force plate and the particles, making the mechanical response of the force plate particularly inelastic. In these cases, we expect the observed λ ($\sim$0.13) by Gimbert et al. (2019) to apply to our work.

The particle density ρ_s and the soil's scattering damping factor ξ are also associated with uncertainties. However, ρ_s is not expected to vary enough between events in order to provide the increase in predicted basal force fluctuations, which would compensate for missing frontal peaks of the events on 1 July and 2 July 2019. Similarly, ξ varies little unless bedrock is exposed (Kean et al., 2015), which is not the case on the Illgraben debris fan.

6. Conclusions

In this study we analyzed force plate data with high temporal resolution, and seismic and flow depth measurements in the Illgraben torrent (CH), to investigate the generation of fluctuating basal forces during debris flows. We extended the work by Zhang et al. (2021) to use high frequency seismic signals to invert the debris-flow basal fluctuating forces. These seismically derived fluctuating basal forces match well with the measured basal force fluctuations at a force plate, though we were unable to invert the absolute amplitude of basal force fluctuations due to the unconstrained surface area of the seismic signal's source region and the simplification of the seismic ground model. We observe that the bulk characteristics (weight and flow depth) of the debris flow are related to the seismically derived basal fluctuating forces and the measured basal force fluctuations, which implies that high frequency seismic signals can be used to extract the debris-flow bulk characteristics.

In order to quantitatively explain the relation between the high frequency seismic signal generated by the debris flows and the flows' bulk characteristics, we propose a new physical model in which a high frequency seismic signal is generated by the impact forces of multi-particle force chains and of individual particles, within a debris flow. In the cases in which only single particles or only force chains undergo impacts, the exponents of flow depth in our model's expression for basal force fluctuations are 1.22 and 2.22, respectively. We observe that the flow depth dependence of the basal force fluctuations for all events is within this predicted flow depth dependence range, which is also similar to the measurements from other debris-flow torrent (Coviello et al., 2019) and flume (Allstadt et al., 2020) experiments. This suggests that in order to predict debris-flow basal force fluctuations,

the random single-particle impacts and the random impacts of multi-particle force chains need to be considered simultaneously, because these two mechanisms are active at the same time. Furthermore, for different events and different instances within an event, the relative contributions of single particles and of multi-particle force chains vary significantly. The relative contribution of multi-particle force chains is expected to be larger in the flow front, where particle concentrations are higher. As the flow depth and/or the concentration of coarse particles decrease in the flow, the relative contribution of multi-particle force chains decreases. We have observed that a reasonable η reflecting the relative contributions of single particles and of multi-particle force chains can significantly improve predictions of the debris-flow's basal force fluctuation, though the exact value of η is generally difficult to constrain.

Data Availability Statement

The data from the Illgraben network is collected under the network code XP, https://doi.org/10.12686/sed/networks/xp, and all seismic data are openly available after a 1-year embargo (in 2022) via the Swiss Seismological Service, http://arclink.ethz.ch/webinterface, and the European Integrated Data Archive (EIDA), http://www.orfeus-eu.org/data/eida. Force plate measurements, flow depth data and boulder data are available at https://doi.org/10.3929/ethz-b-000437719. The data in Figure 9 was reused from Coviello et al. (2019) with permission from John Wiley and Sons.

Acknowledgments
We thank Rachel Abercrombie, Victor Tsai, and Matthew Arran for their thoughtful remarks and for reviews, which significantly improved the quality of this manuscript. Seismometer deployments were funded by WSL and the Canton Valais and supported by the Swiss Military. We thank the Swiss Seismological Service and its electronic laboratory (ELAB) for technical support. This work was supported by the National Key Research and Development program of China (Project No. 2017YFC1501003), the Major Program of the National Natural Science Foundation of China (Grant No. 41790433), the National Natural Science Foundation of China (Grant No. 41772312), and the Project of China Railway Eryuan Engineering Group Co. Ltd (Grant No. K2018G060-1).

References

Allstadt, K. (2013). Extracting source characteristics and dynamics of the August 2010 Mount Meager landslide from broadband seismograms. *Journal of Geophysical Research Earth Surface*, *118*(3), 1472–1490. https://doi.org/10.1002/jgrf.20110

Allstadt, K., Farin, M., Iverson, R. M., Obryk, M. K., Kean, J. W., Tsai, V. C., et al. (2020). Measuring basal force fluctuations of debris flows using seismic recordings and empirical green's functions. *Journal of Geophysical Research: Earth Surface*, *125*, e2020JF005590. https://doi.org/10.1029/2020JF005590

Allstadt, K. E., Matoza, R. S., Lockhart, A., Moran, S. C., Caplan-Auerbach, J., Haney, M., et al. (2018). Seismic and acoustic signatures of surficial mass movements at volcanoes. *Journal of Volcanology and Geothermal Research*, *364*, 76–106. https://doi.org/10.1016/j.jvolgeores.2018.09.007

Arran, M. I., Mangeney, A., De Rosny, J., Farin, M., Toussaint, R., & Roche, O. (2021). Laboratory landquakes: Insights from experiments into the high-frequency seismic signal generated by geophysical granular flows. *Journal of Geophysical Research: Earth Surface*, *126*, e2021JF006172. https://doi.org/10.1029/2021JF006172

Badoux, A., Graf, C., Rhyner, J., Kuntner, R., & McArdell, B. W. (2009). A debris-flow alarm system for the Alpine Illgraben catchment: Design and performance. *Natural Hazards*, *49*(3), 517–539. https://doi.org/10.1007/s11069-008-9303-x

Behringer, R. P., Dapeng, B., Charkraborty, B., Henkes, S., & Hartley, R. R. (2008). Why do granular materials stiffen with shear rate? Test of novel stress-based statistics, *Physical Review Letters*, *101*, 268301. https://doi.org/10.1103/PhysRevLett.101.268301

Campbell, C. S. (2006). Granular material flows– An overview. *Powder Technology*, *162*(3), 208–229. https://doi.org/10.1016/j.powtec.2005.12.008

Chmiel, M., Walter, F., Wenner, M., Zhang, Z., McArdell, B., Clinton, J., & Hibert, C. (2021). Machine learning improves debris flow warning. *Geophysical Research Letters*, *48*(3), e2020GL090874. https://doi.org/10.1029/2020GL090874

Coviello, V., Arattano, M., Comiti, F., Macconi, P. & Marchi, L. (2019). Seismic characterization of debris flows: Insights into energy radiation and implications for warning, *Journal of Geophysical Research Earth Surface*, *124*(6), 1440–1463. https://doi.org/10.1029/2018jf004683

de Haas, T., Aberg, A. S., Walter, F., & Zhang, Z. (2021). Deciphering seismic and normal-force fluctuation signatures of debris flows: An experimental assessment of effects of flow composition and dynamics. *Earth Surface Processes and Landforms*, *46*, 2195–2210. https://doi.org/10.1002/esp.5168

Durda, D. D., Movshovitz, N., Richardson, D. C., Asphaug, E., Morgan, A., Rawlings, A. R., & Vest, C. (2011). Experimental determination of the coefficient of restitution for meter-scale granite spheres. *Icarus*, *211*(1), 849–855. https://doi.org/10.1016/j.icarus.2010.09.003

Ekström, G., & Stark, C. P. (2013). Simple scaling of catastrophic landslide dynamics. *Science*, *339*(6126), 1416–1419. https://doi.org/10.1126/science.1232887

Estep, J., & Dufek, J. (2012). Substrate effects from force chain dynamics in dense granular flows. *Journal of Geophysical Research: Earth Surface*, *117*(F1), F01028. https://doi.org/10.1029/2011JF002125

Farin, M., Tsai, V. C., Lamb, M. P., & Allstadt, K. E. (2019). A physical model of the high-frequency seismic signal generated by debris flows. *Earth Surface Processes and Landforms*, *44*(13), 2529–2543. https://doi.org/10.1002/esp.4677

Furbish, D. J., Schmeeckle, M. W., & Roering, J. J. (2008). Thermal and force-chain effects in an experimental, sloping granular shear flow. *Earth Surface Processes and Landforms*, *33*(13), 2108–2117. https://doi.org/10.1002/esp.1655

Gimbert, F., Fuller, B. M., Lamb, M. P., Tsai, V. C., & Johnson, J. (2019). Particle transport mechanics and induced seismic noise in steep flume experiments with accelerometer-embedded tracers. *Earth Surface Processes and Landforms*, *44*, 21–241. https://doi.org/10.1002/esp.4495

Gimbert, F., Tsai, V. C., & Lamb, M. P. (2014). A physical model for seismic noise generation by turbulent flow in rivers. *Journal of Geophysical Research: Earth Surface*, *119*, 2209–2238. https://doi.org/10.1002/2014JF003201

Hertz, H. (1882). Ueber die Berührung fester elastischer Körper. *Journal fur die Reine und Angewandte Mathematik*, *92*, 156–171. https://doi.org/10.1515/9783112342404-004

Hibert, C., Ekström, G., & Stark, C. P. (2017). The relationship between bulk-mass momentum and short-period seismic radiation in catastrophic landslides: Landslides short-period seismic signals. *Journal of Geophysical Research Earth Surface*, *122*(5), 1201–1215. https://doi.org/10.1002/2016jf004027

Hsu, L., Dietrich, W. E., & Sklar, L. S. (2014). Mean and fluctuating basal forces generated by granular flows: Laboratory observations in a large vertically rotating drum. *Journal of Geophysical Research: Earth Surface*, *119*(6), 1283–1309. https://doi.org/10.1002/2013JF003078

Hungr, O. (1995). A model for the runout analysis of rapid flow slides, debris flows, and avalanches. *Canadian Geotechnical Journal*, *32*(4), 610–623. https://doi.org/10.1139/t95-063

Hungr, O., Morgan, G. C., & Kellerhals, R. (1984). Quantitative analysis of debris torrent hazards for design of remedial measures. *Canadian Geotechnical Journal*, *21*(4), 663–677. https://doi.org/10.1139/t84-073

Hürlimann, M., Rickenmann, D., & Graf, C. (2003). Field and monitoring data of debris-flow events in the Swiss Alps. *Canadian Geotechnical Journal*, *40*(1), 161–175. https://doi.org/10.1139/t02-087

Iverson, R. M. (1997). The physics of debris flows. *Reviews of Geophysics*, *35*(3), 245–296. https://doi.org/10.1029/97RG00426

Iverson, R. M., & LaHusen, R. G. (1989). Dynamic pore-pressure fluctuations in rapidly shearing granular materials. *Science*, *246*(4931), 796–799. https://doi.org/10.1126/science.246.4931.796

Jackson, R. L., Green, I., & Marghitu, D. B. (2010). Predicting the coefficient of restitution of impacting elastic-perfectly plastic spheres. *Nonlinear Dynamics*, *60*(3), 217–229. https://doi.org/10.1007/s11071-009-9591-z

Johnson, C. G., Kokelaar, B. P., Iverson, R. M., Logan, M., LaHusen, R. G., & Gray, J. M. N. T. (2012). Grain-size segregation and levee formation in geophysical mass flows. *Journal of Geophysical Research*, *117*, F01032. https://doi.org/10.1029/2011JF002185

Johnson, K. L. (1987). *Contact mechanics* (p. 452). Cambridge University Press.

Kean, J., Coe, J., Coviello, V., Smith, J., McCoy, S., & Arattano, M. (2015). Estimating rates of debris flow entrainment from ground vibrations. *Geophysical Research Letters*, *42*, 6365–6372. https://doi.org/10.1002/2015GL064811

Lai, V. H., Tsai, V. C., Lamb, M. P., Ulizio, T. P., & Beer, A. R. (2018). The seismic signature of debris flows: Flow mechanics and early warning at Montecito, California. *Geophysical Research Letters*, *45*, 5528–5535. https://doi.org/10.1029/2018gl077683

Lamb, M. P., Dietrich, W. E., & Sklar, L. S. (2008). A model for fluvial bedrock incision by impacting suspended and bed load sediment. *Journal of Geophysical Research*, *113*, F03025. https://doi.org/10.1029/2007JF000915

Majmudar, T. S., & Behringer, R. P. (2005). Contact force measurements and stress-induced anisotropy in granular materials. *Nature*, *435*, 1079–1082. https://doi.org/10.1038/nature03805

Majmudar, T. S., Sperl, M., Luding, S., & Behringer, R. P. (2007). Jamming transition in granular systems. *Physical Review Letters*, *98*, 058001. https://doi.org/10.1103/physrevlett.98.058001

McArdell, B. W., Bartelt, P., & Kowalski, J. (2007). Field observations of basal forces and fluid pore pressure in a debris flow. *Geophysical Research Letters*, *34*, L07406. https://doi.org/10.1029/2006gl029183

McCoy, S. W., Tucker, G. E., Kean, J. W., & Coe, J. A. (2013). Field measurement of basal forces generated by erosive debris flows. *Journal of Geophysical Research: Earth Surface*, *118*(2), 589–602. https://doi.org/10.1002/jgrf.20041

Muthuswamy, M., & Tordesillas, A. (2006). How do interparticle contact friction, packing density, and degree of polydispersity affect force propagation in particulate assemblies? *Journal of Statistical Mechanics*, *2006*, P09003. https://doi.org/10.1088/1742-5468/2006/09/P09003

Ogiso, M., & Yomogida, K. (2015). Estimation of locations and migration of debris flows on Izu-Oshima Island, Japan, on 16 October 2013 by the distribution of high frequency seismic amplitudes. *Journal of Volcanology and Geothermal Research*, *298*, 15–26. https://doi.org/10.1016/j.jvolgeores.2015.03.015

Pierson, T. C. (1986). Flow behavior of channelized debris flows, Mount St. Helens, Washington. In A. D. Abrahams (Ed.), *Hillslope processes* (pp. 269–296). Allen & Unwin. Boston.

Rickenmann, D. (1999). Empirical relationships for debris flows. *Natural Hazards*, *19*, 47–77. https://doi.org/10.1023/a:1008064220727

Rickenmann, D., Turowski, J. M., Fritschi, B., Klaiber, A., & Ludwig, A. (2012). Bedload transport measurements at the Erlenbach stream with geophones and automated basket samplers. *Earth Surface Processes and Landforms*, *37*(9), 1000–1011. https://doi.org/10.1002/esp.3225

Schimmel, A., & Hübl, J. (2015). Approach for an early warning system for debris flows based on acoustic signals. In G. Lollino, M. Arattano, M. Rinaldi, O. Giustolisi, J. C. Marechal, & G.Grant, (Eds.), *Engineering geology for society and territory* (Vol. 3, pp. 55–58). Springer. https://doi.org/10.1007/978-3-319-09054-2_11

Schimmel, A., & Hübl, J. (2016). Automatic detection of debris flows and debris floods based on a combination of infrasound and seismic signals. *Landslides*, *13*(5), 1181–1196. https://doi.org/10.1007/s10346-015-0640-z

Schlunegger, F., Badoux, A., McArdell, B. W., Gwerder, C., Schnydrig, D., Rieke-Zapp, D., & Molnar, P. (2009). Limits of sediment transfer in an alpine debris-flow catchment, Illgraben, Switzerland. *Quaternary Science Reviews*, *28*, 1097–1105. https://doi.org/10.1016/j.quascirev.2008.10.025

Schmandt, B., Aster, R. C., Scherler, D., Tsai, V. C., & Karlstrom, K. (2013). Multiple fluvial processes detected by riverside seismic and infrasound monitoring of a controlled flood in the Grand Canyon. *Geophysical Research Letters*, *40*, 4858–4863. https://doi.org/10.1002/grl.50953

Silbert, L. E., Ertass, D., Grest, G. S., Halsey, T. C., Levine, D., & Plimpton, S. J. (2001). Granular flow down an inclined plane: Bagnold scaling and rheology. *Physical Review E*, *64*, 051302. https://doi.org/10.1103/PhysRevE.64.051302

Thomas, A. L., & Vriend, N. M. (2019). Photoelastic study of dense granular free-surface flows. *Physical Review E*, *100*, 012902. https://doi.org/10.1103/PhysRevE.100.012902

Tsai, V. C., Minchew, B., Lamb, M. P., & Ampuero, J.-P. (2012). A physical model for seismic noise generation from sediment transport in rivers. *Geophysical Research Letters*, *39*(2), L02404. https://doi.org/10.1029/2011GL050255

Viroulet, S., Baker, J. L., Rocha, F. M., Johnson, C. G., Kokelaar, B. P., & Gray, J. M. N. T. (2018). The kinematics of bidisperse granular roll waves. *Journal of Fluid Mechanics*, *848*, 836–875. https://doi.org/10.1017/jfm.2018.348

Walter, F., Amann, F., Kos, A., Kenner, R., Phillips, M., de Preux, A., et al. (2020). Direct observations of a three million cubic meter rock-slope collapse with almost immediate initiation of ensuing debris flows. *Geomorphology*, *351*, 106933. https://doi.org/10.1016/j.geomorph.2019.106933

Walter, F., Burtin, A., McArdell, B. W., Hovius, N., Weder, B., & Turowski, J. M. (2017). Testing seismic amplitude source location for fast debris-flow detection in Illgraben, Switzerland. *Natural Hazards and Earth System Sciences*, *17*(6), 939–955. https://doi.org/10.5194/nhess-17-939-2017

Zhang, Z., & He, S. (2019). Analysis of broadband seismic recordings of landslide using empirical Green's function. *Geophysical Research Letters*, *46*(9), 4628–4635. https://doi.org/10.1029/2018GL081448

Zhang, Z., Walter, F., McArdell, B. W., Wenner, M., Chmiel, M., de Haas, T., & He, S. (2021). Insights from the particle impact model into the high frequency seismic signature of debris flows. *Geophysical Research Letters*, *48*, e2020GL088994. https://doi.org/10.1029/2020GL088994

References From the Supporting Information

Aki, K., & Richards, P. G. (2002). *Quantitative seismology* (2nd ed.). University Science Books.

Arai, H., & Tokimatsu, K. (2004). S-wave velocity profiling by inversion of microtremor H/V spectrum. *Bulletin of the Seismological Society of America*, *94*(1), 53–63. https://doi.org/10.1785/0120030028

Harkrider, D. G. (1964). Surface waves in multilayered elastic media I. Rayleigh and Love waves from buried sources in a multilayered elastic half-space. *Bulletin of the Seismological Society of America*, *54*(2), 627–679. https://doi.org/10.1785/bssa0540020627